JOURNAL OF GEOPHYSICAL RESEARCH, VOL. 98, NO. C8, PAGES 14,651–14,668, AUGUST 15, 1993

Wind Field Model-Based Estimation of Seasat Scatterometer Winds

DAVID G. LONG

Electrical and Computer Engineering Department, Brigham Young University, Provo, Utah

A model-based approach to estimating near-surface wind fields over the ocean from Seasat scatterometer (SASS) measurements is presented. The approach is a direct assimilation technique in which wind field model parameters are estimated directly from the scatterometer measurements of the radar backscatter of the ocean's surface using maximum likelihood principles. The wind field estimate is then computed from the estimated model parameters. The wind field model used in this approach is based on geostrophic approximation and on simplistic assumptions about the wind field vorticity and divergence but includes ageostrophic winds. Nine days of SASS data were processed to obtain unique wind estimates. Comparisons in performance to the traditional two-step (point-wise wind retrieval followed by ambiguity removal) wind estimate method and the model-based method are provided using both simulated radar backscatter measurements and actual SASS measurements. In the latter case the results are compared to wind fields determined using subjective ambiguity removal. While the traditional approach results in missing measurements and reduced effective swath width due to fore/aft beam cell coregistration problems, the model-based approach uses all available measurements to increase the effective swath width and to reduce data gaps. The results reveal that the model-based wind estimates have accuracy comparable to traditionally estimated winds with less "noise" in the directional estimates, particularly at low wind speeds. In addition, wind fields generated using the model-based procedure can be used to detect and correct ambiguity removal errors in ambiguity-removed point-wise wind fields. A separate procedure, based only on the wind field model, can also be used as a data quality check to detect errors in point-wise ambiguity removal.

1. INTRODUCTION

From measurements of the normalized radar backscatter (σ^0) made by the Seasat scatterometer (SASS) the near-surface wind over the ocean can be inferred using a geophysical model function relating σ^0 and the vector wind (see, for example, *Freilich* [1986], *Jones et al.* [1982], *Ulaby et al.* [1981], and *Wentz et al.* [1984]). Previously, a point-wise approach has been used to retrieve SASS winds. In point-wise wind retrieval, only the σ^0 measurements corresponding to a particular sample point are used to estimate the wind at that sample point. Because of the biharmonic nature of the geophysical model function (the upwind σ^0 is similar in value to the downwind σ^0) the wind estimate is not unique; that is, there are several wind vectors which "explain" the measurements. These vectors have similar magnitude but quite different directions. To obtain a single wind vector estimate, an ambiguity removal (sometimes termed "alias removal" or "dealiasing" in the literature) procedure is required. Ambiguity removal algorithms are typically based on ad hoc considerations or pattern recognition and tend to be very error-prone [*Schroeder et al.*, 1985; *Shaffer et al.*, 1991; *Wurtele et al.*, 1982]. While model-based ambiguity selection algorithms have been developed [e.g., *Atlas et al.*, 1987; *Hoffman*, 1982], these have some of the same limitations as other alias removal techniques. Instead, in this paper a model-based wind retrieval technique is used.

The model-based wind retrieval method estimates the wind field over the entire swath by estimating the parameters of a model of the underlying wind field directly from the measurements of σ^0; that is, the σ^0 measurements are assimilated directly into the wind field model. This approach can result in more accurate estimates of the wind over a wider swath with fewer holes than point-wise estimates. While point-wise wind estimates can be used to initialize the model-based retrieval in order to save computation, point-wise ambiguity removal is not a requirement. Additionally, the wind field divergence and vorticity are directly estimated as part of the model-based wind retrieval process.

The feasibility of model-based wind retrieval for simulated NASA scatterometer (NSCAT) measurements was first shown by *Long and Mendel* [1990*a*, *b*]. In this paper the method is applied to SASS data. A comparison of the wind estimation performance of model-based and traditional wind retrieval is provided. The relative advantages and limitations of the method are considered in detail with illustrative examples given. Nine days of SASS data for which subjective ambiguity removal is available [*Wurtele et al.*, 1982] were processed using the model-based wind retrieval technique. Detailed comparisons between the resultant wind fields were made. The results demonstrate the utility of the technique for SASS wind retrieval.

Paper number 93JC01290.
0148-0227/93/93JC-01290$05.00

2. POINT-WISE WIND RETRIEVAL USING SASS σ^0 MEASUREMENTS

SASS made 14.6-GHz measurements of σ^0 at two azimuth angles 90° apart over a 500-km swath on each side of the spacecraft ground track [*Grantham et al.*, 1982]. Because of the often low signal-to-noise ratios (SNR) the σ^0 measurements were noisy. In addition, the swath width covered by each antenna varied along the orbit owing to the effects of Earth's rotation on the resolution-creating Doppler filters which resulted in misregistration of the σ^0 measurements made by the fore- and aft-looking antennas [*Naderi et al.*, 1991]. Multiple measurements of σ^0 from different azimuth angles are required to retrieve the wind in point-wise wind retrieval; this results in a narrowing of the effective wind measurement swath and numerous "holes" or missing measurements in the estimated wind fields.

While the actual SASS measurements fall on an irregular

grid, for the purposes of this study the SASS measurements were binned into a 50-km resolution grid. Each σ^0 measurement was assigned to the single grid element in which the σ^0 measurement center was located. The binned measurements are treated as if they were located at the grid element centers. The error introduced by this approximation is considered negligible. We note that modern scatterometers such as ERS 1 and the future NSCAT are designed to insure that the σ^0 measurements will fall on a regular grid. While some previous investigators [e.g., *Wurtele et al.*, 1982] have resampled the σ^0 measurements onto a lower-resolution 100-km grid for point-wise wind retrieval, in this work a 50-km grid is used.

In point-wise wind retrieval, only the σ^0 measurements associated with a single grid element are used to retrieve the wind for that grid element. For those grid elements for which point-wise wind retrieval can be performed, there are from two to four wind vector ambiguities (sometimes termed "aliases" in the literature) with similar speed but quite different directions. For point-wise wind retrieval with only two azimuth angle observations of σ^0 there is insufficient information in the σ^0 measurements to indicate which of these vector ambiguities corresponds to the "true" wind; that is, it is impossible to select a unique wind direction from the σ^0 measurements at a single grid element alone; they are all equally viable solutions. Note that this would be true even if the σ^0 measurements were noise free [*Long and Mendel*, 1991]. Thus, to select a unique wind vector, additional information must be used. In traditional wind retrieval this information is provided by looking at nearby wind estimates and employing pattern recognition or other techniques [*Schroeder et al.*, 1985; *Wurtele et al.*, 1982]. Modern scatterometers incorporate an additional antenna to make an additional azimuthal measurement of σ^0. This additional measurement provides some "skill" in selecting a unique wind vector estimate [see *Long and Mendel*, 1991; *Schroeder et al.*, 1985]. However, multiple solutions still occur even in this case. Further, the added "skill" depends on the swath location and the wind speed resulting in ambiguity removal errors which are correlated with the wind field [e.g., *Shaffer et al.*, 1991].

Using point-wise wind retrieval, a wind estimate can be made only for those grid points for which there are σ^0 measurements from both the fore- and aft-facing antenna beams. If measurements from only a single azimuth angle are available at a given grid point, the σ^0 measurements are effectively discarded, resulting in "holes" in the estimated wind field. This also leads to the narrowing of the SASS wind estimate for point-wise estimation because of the misregistration of the σ^0 measurements from the fore- and aft-facing antennas. For model-based wind retrieval, however, the wind field can be retrieved even when there are some missing σ^0 measurements; hence there are fewer data gaps and a wider swath in the retrieved fields.

3. WIND FIELD MODEL

The model-based wind retrieval method is based on the direct assimilation of the σ^0 into a model for the wind field. The model provides a description of the near-surface wind field over the scatterometer measurement swath at a fixed instant of time and a resolution of 50 km (corresponding to the SASS spatial sampling). In model-based estimation the model provides constraints for the wind estimate derived from the σ^0 measurements. These constraints result in reduced "noise" in the estimated wind while eliminating the requirement for point-wise ambiguity removal.

In this section the wind field model is derived. In developing the model, formulations which would require data other than those from the scatterometer were avoided. While this is a limiting factor in the modeling accuracy, it permits the model to be employed even in the absence of any other supporting data. However, as described below, some external data may be required to resolve potential ambiguity in the model-based wind retrieval procedure. We restrict our attention to a limited-area region with a maximum spatial extent of approximately 500 km, corresponding to the swath width of the scatterometer.

Denoting the near-surface horizontal wind field of interest by $\mathbf{U} = (u, v)^T$, the vorticity ζ and divergence δ of $\mathbf{U}$ may be defined as

$$\zeta = \mathbf{k} \cdot \nabla \times \mathbf{U} \tag{1}$$

$$\delta = \nabla \cdot \mathbf{U}, \tag{2}$$

where $\mathbf{k}$ is a unit vector in the vertical direction.

Using the Helmholtz theorem, $\mathbf{U}$ may be defined by a stream function ψ and velocity potential χ according to [see *Bijlsma et al.*, 1986; *Lynch*, 1988]

$$\mathbf{U} = \mathbf{k} \times \nabla\psi + \nabla\chi, \tag{3}$$

where $\mathbf{k} \times \nabla\psi$ is a nondivergent vector field and $\nabla\chi$ is a curl-free vector field.

Taking the divergence and curl, respectively, of (3), we obtain Poisson equations for ψ and χ,

$$\nabla^2\psi = \zeta \tag{4}$$

$$\nabla^2\chi = \delta. \tag{5}$$

For reconstructing a wind field from specified vorticity and divergence, *Lynch* [1988] has argued that the reconstruction is not unique over a limited domain; an arbitrary harmonic function may be added to χ, provided ψ is also altered, to produce the same wind field. From this he concludes that the boundary values of χ may be set arbitrarily. He shows that setting the boundary values of χ to zero minimizes the divergent component of the kinetic energy and that choosing $\chi = 0$ on the boundary ensures a unique reconstruction of the wind field. Following this line of reasoning, we set $\chi = 0$ on the region boundary. Thus we assume (on scales from 50 to 500 km) that the wind field has minimum divergent kinetic energy. By assuming $\chi = 0$ on the boundary (equations (4) and (5)) the vorticity and divergence fields and the boundary conditions for ψ completely describe the wind vector field.

To obtain simple boundary conditions for ψ, a second assumption attributes ψ to the geostrophic motion, that is, that the stream function ψ is proportional to the geostrophic pressure field p,

$$\psi = \frac{1}{\rho f} p, \tag{6}$$

where ρ is the density and f is the Coriolus parameter. Note that in a strictly geostrophic formulation the wind field would

be nondivergent and χ would be identically zero. In the more general formulation which we will adopt, χ corresponds to the ageostrophic component of the wind.

By making these assumptions the boundary values for (4) and (5) can be specified in terms of the geostrophic pressure field. This avoids the difficulties of using velocity boundary conditions which may yield an overdetermined system [*Lynch*, 1988].

A third modeling assumption is that over the region of interest, ρf is essentially constant (i.e., an f plane approximation with constant ρ). We can then normalize the pressure field by ρf so that $\psi = p$; that is, ψ is then the normalized geostrophic pressure field. While in principle, this can lead to difficulty in applying the model near the equator, in practice, the model can still be applied [cf. *Yu*, 1987]. Equation (3) can be written in component form as

$$u = -\frac{\partial p}{\partial y} + \frac{\partial \chi}{\partial x} \tag{7}$$

$$v = \frac{\partial p}{\partial x} + \frac{\partial \chi}{\partial y}. \tag{8}$$

Equations (7) and (8), along with (4) and (5) form the basis of the wind field model.

To complete the wind field model, models for the vorticity and divergence fields are needed. Without requiring auxiliary data, usable dynamic models for these fields over the scales of interest are difficult to formulate. Instead, we adopt a descriptive modeling approach by assuming that the vorticity and divergence fields are relatively smooth and can be adequately described by low-order bivariate polynomials over the region of interest. Such an approach, while not physically based, produces a model of adequate accuracy for use in scatterometer wind retrieval. However, the assumed form for the vorticity and divergence field models limits the ability of the final model to accurately describe fronts. This limitation will be discussed further in section 4.7. For this paper the following bivariate forms for the vorticity and divergence fields are used:

$$\zeta(x, y) = \sum_{\substack{m=0 \\ m+n \le M_C}}^{M_C} \sum_{n=0}^{M_C} c_{m,n} x^m y^n \tag{9}$$

$$\delta(x, y) = \sum_{\substack{m=0 \\ m+n \le M_D}}^{M_D} \sum_{n=0}^{M_D} d_{m,n} x^m y^n \tag{10}$$

where M_C and M_D are the model orders and $c_{m,n}$ and $d_{m,n}$ are the model parameters. The number of parameters in the vorticity and divergence field models is $N_C = (M_C + 1)(M_C + 2)/2$ and $N_D = (M_D + 1)(M_D + 2)/2$, respectively. Selection of M_C and M_D will be discussed later.

Equations (4), (5), and (7)–(10) are discretized on an $M \times N$ rectilinear grid with spacing $h = 50$ km over the desired region corresponding to the 50-km sampling resolution of SASS. M and N represent selectable model parameters (typically, $M = N = 10$). The pressure and velocity potential fields can be eliminated from the discretized system of equations, and the velocity field can be written directly in terms of the pressure field boundary conditions and the parameters of the vorticity and divergence fields. The resulting equation relating the velocity component fields to pressure field boundary conditions and the vorticity and divergence model parameters can be expressed as [*Long*, 1989]

$$\bar{W} = \begin{bmatrix} \bar{U} \\ \bar{V} \end{bmatrix} = F\bar{X} \tag{11}$$

where the MN element vector $\bar{U}$ is the row-ordered u component wind field at grid sample points, $\bar{V}$ is the row-ordered v component wind field, and the $\bar{X}$ vector contains $2M + 2N - 2$ pressure field boundary conditions and $N_C + N_D$ vorticity and divergence field parameters. F is a full-rank rectangular matrix of known constants. $\bar{W}$ is the total wind field.

While not a required part of the model-based estimation method, if we assume that the pressure field boundary conditions are relatively smooth, the number of model parameters can be reduced (at the expense of modeling accuracy) by parameterizing the pressure field boundary conditions using an N_Pth-order periodic function such as low-order Fourier series. This version of the model will be referred to as the PBC model, and the nonparameterized version of the model will be referred to as the NB model. Both models have the form of (11) but the PBC model has slightly different definitions for F and $\bar{X}$ (e.g., $\bar{X}$ is an $N_P + N_C + N_D$ element vector). While the PBC model is somewhat less accurate than the NB model, it is computationally more tractable when used in model-based wind estimation.

4. MODEL-BASED WIND RETRIEVAL

The assimilation approach is based on a simple estimation theory formulation. Equation (11) provides a parametric wind field model which relates the model parameters (in $\bar{X}$) to the wind field (in $\bar{W}$). Using this model, the model parameters are directly estimated from the noisy σ^0 measurements. Estimation of $\bar{X}$ from the noisy σ^0 measurements is done using the maximum likelihood (ML) principle; the negative log likelihood function for the model parameters given the measurements is minimized to estimate the model parameters [*Mendel*, 1973]. The wind field estimate is computed from the estimated model parameters.

The remainder of section 4 describes the details and considerations of the estimation process. Considerations for selecting the wind field model size and order are also discussed.

4.1. *Region Size Considerations*

Unfortunately, minimization of the log likelihood function is computationally intensive; the computation required is inversely proportional to the region area and proportional to a power of the number of unknowns (parameters) in the model. Thus to minimize computation, we minimize the number of model parameters, while maximizing M and N. However, the modeling accuracy decreases with increasing M and N and increases for increasing M_C and M_D. The PBC model, while slightly less accurate than the NB model, requires less computation because it has fewer unknowns. Thus selection of the region size, the model type, and the model orders must be made by trading off modeling accuracy and the computation required [*Long*, 1989].

Selection of the region size is determined primarily by the usable swath width. Misregistration of the σ^0 measurements

from the fore and aft antenna beams limits the swath width for point-wise estimation. However, σ^0 measurements from a single antenna beam are available over a much wider swath [*Grantham et al.*, 1982]. Since multiple azimuthal σ^0 measurements are not required at every grid point, model-based estimation can produce a wider effective wind measurement for SASS than would otherwise be possible with point-wise estimation. When excessive grid points within the model's region of support have missing σ^0 measurements, however, the model-based wind estimate accuracy can deteriorate. Experimentally, it was found that with a region size of $M = 10 \times N = 10$ the effective wind estimate swath can be extended by 100 km beyond the point-wise swath width while maintaining reasonable accuracy along the outer edge of the swath. Thus, in this work a region size of $M = 10 \times N = 10$ (corresponding to 500 × 500 km) was used. Further discussion is reserved for section 5.

In application, each side of the observation swath is segmented into overlapping 500 × 500 km regions. The region overlap is 250 km in the along-track direction. The model-based estimation procedure is applied to each region separately. The wind estimates from each region are averaged where they overlap.

4.2. *ML Objective Function*

At a given sample point with row-ordered index n, the kth observation of σ^0 (denoted by $\sigma_n^0(k)$) will be a function of the true wind vector (u_n, v_n) at the sample point, the observational azimuth and incidence angles, and the polarization; that is;

$$\sigma_n^0(k) = \mathcal{M}\{(u_n, v_n), k\} = \mathcal{M}\{((F\bar{X})_n, (F\bar{X})_{MN+n}), k\}, \quad (12)$$

where $\mathcal{M}\{(u_n, v_n), k\}$ is the value of the geophysical model function for a wind vector (u_n, v_n). The dependence of the model function on the antenna beam and incidence angles and the polarization is subsumed in k. The measurements of σ^0 will be noisy. Let $z_n(k)$ be the noisy measurement $\sigma_n^0(k)$; that is,

$$z_n(k) = \sigma_n^0(k) + \nu_n(k), \quad (13)$$

where $\nu_n(k)$ is a zero-mean, independent Gaussian random variable with variance

$$\text{Var}[z_n(k)] = \alpha_n^2(k)\sigma_n^{02}(k) + \beta_n^2(k)\sigma_n^0(k) + \gamma^2(k), \quad (14)$$

where $\alpha_n(k)$, $\beta_n(k)$, and $\gamma(k)$ depend on the measurement geometry and the scatterometer design (see *Long and Mendel* [1991] for further discussion). The conditional probability density of $z_n(k)$ given $\bar{X}$ is then

$$p(z_n(k)|\bar{X}) = \frac{1}{(2\pi)^{1/2}} \frac{1}{\{\text{Var}[z_n(k)]\}^{1/2}} \exp\{-\tfrac{1}{2}[z_n(k) - \sigma_n^0(k)]^2/\text{Var}[z_n(k)]\}, \quad (15)$$

where $\sigma_n^0(k)$ is given by (12). The log likelihood function $l(\bar{X})$ for $\bar{X}$ given all the measurements $z_n(k)$ is then

$$l(\bar{X}) = \sum_{n=1}^{N^2} \sum_{k=1}^{L_n} \log p(z_n(k)|\bar{X}). \quad (16)$$

Disregarding any constants, $l(\bar{X})$ can be written as

$$l(\bar{X}) = -\sum_{n=1}^{N^2} \sum_{k=1}^{L_n} \{\log\{\text{Var}[z_n(k)]\} + [z_n(k) - \sigma_n^0(k)]^2/\text{Var}[z_n(k)]\}, \quad (17)$$

where $\sigma_n^0(k)$ is given by (12) and $\text{Var}[z_n(k)]$ is given by (14). We define the ML objective function $J(\bar{X})$ as the negative of the log likelihood function. The ML estimate of $\bar{X}$ is obtained by minimizing $J(\bar{X})$.

4.3. *Computation of the ML Estimate of* $\bar{X}$

Since $\mathcal{M}$ is a tabular function, a closed form for the minimum of $J(\bar{X})$ is not available; hence $J(\bar{X})$ must be numerically optimized. Unfortunately, the objective function can be difficult to optimize due to the dimensionality of the problem and the nonlinear properties it inherits from the nature of $\mathcal{M}$. In particular, the objective function has numerous local minima with the possibility of several global minima.

Classic nonlinear minimization algorithms include stochastic algorithms such as simulated annealing and various gradient search techniques. While random optimization techniques are able to locate global minima using multiple restarts, they may require an excessive number of function evaluations to find even a single global minimum. While gradient-based optimization algorithms can get stuck in a local minimum and fail to find a global minimum, multiple optimizations which start with different initial values can be used to find multiple global minima. As a result, gradient search algorithms can be used successfully provided appropriate initial values can be determined.

While alternate initial value computation schemes which do not use the point-wise estimated winds can be used [*Long*, 1989], point-wise estimated winds can be used to simplify the computation of suitable initial values. Two methods for computing initial values from the point-wise estimates were developed. The first, termed FIT, is based on fitting the wind field model to the wind vector field generated by conventional point-wise wind retrieval and ambiguity removal. The second, termed MINIT, uses the point-wise wind speed estimates (but not directions) and does not require ambiguity removal. Both methods are described below. Given an initial value, the nonlinear optimization routine IMING (which uses a quasi-Newton method) from International Mathematics and Statistics Libraries is used to minimize $J(\bar{X})$.

4.4. *Initial Value Computation*

To compute an initial value from the ambiguity removal-selected point-wise wind field using the FIT method, a least squares fit of the model to the selected ambiguity field is computed. Let $\bar{W}'$ be the selected ambiguity field with missing wind estimates filled with the average of nearby estimates. Then an initial estimate $\bar{X}'$ is computed:

$$\bar{X}' = F^{\dagger}\bar{W}', \quad (18)$$

where $F^{\dagger} = (F^TF)^{-1}F^T$ is the pseudoinverse of F. A single initial value is provided by this method for a given selected ambiguity field. While the quality of the FIT-computed initial

value is dependent on the accuracy of the ambiguity removal, the resultant wind estimate is tolerant of sparsely occurring ambiguity removal errors. Thus, in practice, FIT generally results in a good wind estimate. However, when there are a large number of ambiguity selection errors in the region, a poor quality initial value may result, leading to convergence to a local minimum or to lack of convergence of the gradient search algorithm. In this event the wind field estimate may be poor. As shown below, however, such occurrences are rare.

The second initial value computation method, MINIT, utilizes only the wind speed information from the point-wise wind estimates and so does not require point-wise ambiguity removal. It provides multiple initial values. To apply this method, the average wind speed of the point-wise ambiguities is first determined for each grid point. A specialized gradient search algorithm, combined with prototype wind direction fields in various patterns and the point-wise wind speeds, is then used to coarsely locate the minima of $J(\bar{X})$. After final optimization with IMING these initial values result in a few distinct estimates. By proper choice of the prototype wind direction fields and the search algorithm parameters this method is virtually always able to locate the (multiple) global minima of $J(\bar{X})$. Because multiple optimizations are used, however, considerably more computation is required for the MINIT initial value computation method than is required for the FIT method. When using the FIT initial value computation method with a second-order PBC model ($N_p = 10$), the model-based wind retrieval approach requires significantly (typically 4–8 times) more computation than does point-wise estimation. Additional computation is required for higher-order models or the NB model. Because the accuracy of the NB and PBC models is similar [*Long*, 1989], the PBC model was primarily used in this work to reduce computation. When the MINIT approach is used with the second-order PBC model, the computation required increases an additional 8–12 times.

4.5. *Identifiability and Estimate Uniqueness*

The estimation theory concept of "identifiability" indicates whether or not an estimated quantity can be uniquely determined from the available measurements [*Mendel*, 1973]. For point-wise estimation it can be shown that the wind vector is set-wise identifiable from the σ^0 measurements and that the wind vector estimate is not unique; that is, several wind vectors (the ambiguities) "explain" the observed σ^0 values [*Long and Mendel*, 1991]. From the measurements at a single point alone a unique wind estimate can not be determined; hence the need for ambiguity removal in which information from other sources (e.g., surrounding measurements) is used to select a single wind direction. For the two azimuth angle SASS, there are two to six ambiguities at each sample point. The precise number depends on the measurement geometry and the true wind vector. Multiple ambiguities also occur for the three azimuth angle ERS-1 scatterometer and NSCAT. Note that this phenomenon is due in part to the geophysical model function's biharmonic dependence on the wind direction in which the upwind σ^0 has nearly the same value as the downwind σ^0. The point-wise case is considered in detail by *Long and Mendel* [1991].

Like point-wise estimation, it can be shown that in model-based estimation $\bar{X}$ is set-wise identifiable from the measurements of σ^0 [*Long*, 1989]. This implies that the estimate of $\bar{X}$ may not be unique; that is, the ML estimate of $\bar{X}$ is a set. However, in order for this set, denoted by D_f^c, to contain multiple members, each of the members of D_f^c must produce different wind fields which have wind vectors at all corresponding sample points which have the same values of $\sigma_n^0(k)$ for all k and n; that is,

$$D_f^c \triangleq \{\bar{X} | \mathcal{M}\{(F\bar{X})_n, k\} = \mathcal{M}\{(F\bar{X}_t)_n, k\} \ \forall n \ \& \ \forall k \in [1, L_n]\}, \quad (19)$$

where $\bar{X}_t$ denotes the true value of $\bar{X}$. This is infrequent for the three azimuth angle NSCAT; however, for the two azimuth angle SASS there are commonly two or more fields for which this occurs. For example, for a given member of D_f^c, the $\bar{X}$ corresponding to a wind field with all the wind directions reversed will generally be a member of D_f^c. Depending on the model order, there are generally no more than six to seven members of D_f^c. Each of these members corresponds to a global minima of $J(\bar{X})$. Unfortunately, from the σ^0 measurements over a single region alone, there is no way to distinguish between these fields, so that selection of a single field requires additional information. To further complicate matters, the measurement noise may introduce additional near-global minima.

4.6. *Field-Wise Ambiguity Removal*

When D_f^c is multimembered, an additional step is required to select a single solution. Such a procedure might be termed "field-wise ambiguity removal" because of its seeming similarity to the "point-wise ambiguity removal" which is always required by the point-wise wind estimation approach. There is, however, a distinct difference between field-wise and point-wise ambiguity removal: in the point-wise case the problem is to choose from two to six possible solutions at each sample point (of which there are MN in an $M \times N$ region), while in the field-wise case, we need only choose between a few possible fields for each region within the measurement swath. Continuity considerations with adjacent and/or overlapping regions greatly simplify field-wise ambiguity selection.

The requirement that the wind estimates for each region be compatible in the area of overlap of the regions dictates the possible combinations of the ambiguous model-based estimates. In this way a small number of feasible wind fields over long (typically several thousand kilometers) along-track segments are determined. Segments are created between land masses and/or regions of very low wind speed where the directional measurement accuracy is low. From the set of feasible wind fields for each segment a single segment is selected based on auxiliary data, for example, forecasts or ship or buoy observations. Alternately, the auxiliary data can be used to select the ambiguous model-based field on a region-by-region basis. Since the point-wise wind estimates determined using subjective ambiguity removal incorporate auxiliary data when available, for this paper we have found it convenient to select the field closest (in a root-mean-square (rms) sense) to the subjective field. For simulations the field closest to the point-wise wind field with ideal ambiguity removal was selected.

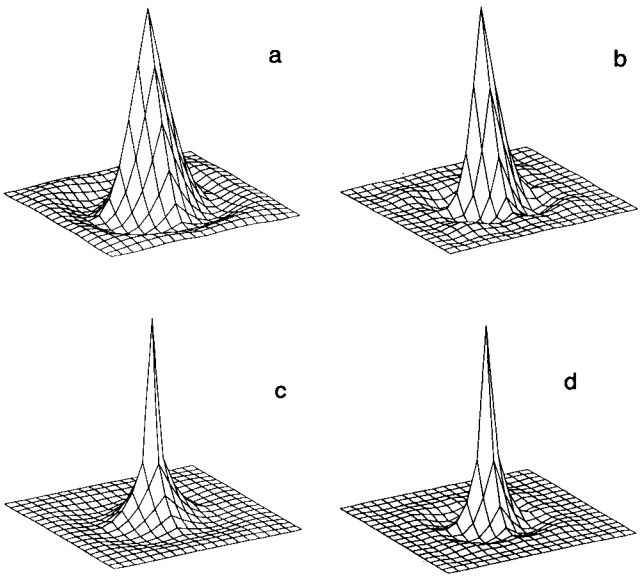

Fig. 1. Plots of the spatial impulse response $\mathcal{F}$ for various model types and orders with size $M = N = 10$. (*a*) PBC model with $N_p = 10$ and $M_C = M_D = 2$. (*b*) PBC model with $N_p = 10$ and $M_C = M_D = 4$. (*c*) NB model with $M_C = M_D = 2$. (*d*) NB model with $M_C = M_D = 4$.

4.7. *Model Order and Smoothing*

The modeling approach used in this paper is based on a geostrophic approximation (with some generalization for ageostrophic winds) and does not explicitly include fronts which exhibit wide changes in speed and direction on small spatial scales. As a result these features can not be accurately described by the model and will be "smoothed" in the estimated wind fields. Note, however, that the inherent scatterometer resolution is ~50 km with inherent under sampling of very small scale wind field features and fronts. Such features will tend to be smoothed even for idealized wind retrieval. This may be desirable in order to remove cloud divergence effects [see *Overland and Wilson*, 1984].

In model-based wind retrieval, additional smoothing arises as a result of the smoothing of the vorticity and divergence fields due to the low-order polynomial approximation. Smoothing of the vorticity and divergence fields results, in turn, in smoothing of the wind field. In addition, the PBC model has additional smoothing due to the boundary conditions parameterization. Increasing the model orders of the vorticity and divergence fields (and, for the PBC model, the boundary condition parameterization) decreases the smoothing and hence the modeling error. However, increasing the model order also increases the computation required to optimize the ML objective function; hence selection of the wind field model order requires a trade-off between the accuracy of the wind field model and computational requirements.

To study the modeling error, consider the wind field model as given by (11). For a given input wind field a least squares fit of the model to the wind field can be computed using (18) with the model fit wind field, $\bar{W}_m$, computed using (11), i.e.,

$$\bar{W}_m = FF^{\dagger}\bar{W}. \tag{20}$$

The resulting error in the wind field is

$$\bar{W}_e = \bar{W} - \bar{W}_m = (I - FF^{\dagger})\bar{W}. \tag{21}$$

We note that only components of $\bar{W}$ which are in the null space of $FF^{\dagger}$ will appear in $\bar{W}_e$. Wind fields in the range space can be exactly represented by the model and will not result in error.

There are a variety of ways of quantifying the modeling error. In this paper we consider a very simple approach based on a wavenumber analysis. Equation (21) describes the wind field modeling error over a single $M \times N$ region. In actual application, regions are overlapped, and the resulting estimates are averaged. For sufficient overlap this process can be viewed as the discrete convolution of the sampled wind field and a model kernel, termed $\mathcal{F}$, which may be computed from $FF^{\dagger}$ by shifting and adding. (Because of the complexity of this computation, the details are not given here.) Then $\mathcal{F}$ can be viewed as the spatial impulse response of the model (see Figure 1).

A slice of the wavenumber response (the magnitude discrete Fourier transform of $\mathcal{F}$) is plotted in Figure 2. As evident from this plot, the model attenuates high wavenumber features in the wind field which have scale lengths less than 200–250 km depending on the model order and type. This is only slightly above the Nyquist sampling cutoff scale length of 100 km. However, only wind field features not in the range space of the model, such as fronts, are affected. Although fronts and very small scale wind features are attenuated, they remain visible in the estimated wind fields, as will be illustrated below.

4.8. *Ambiguity Removal Quality Control Using the Wind Field Model*

One difficulty with traditional ambiguity removal algorithms has been in providing data quality estimates for the estimated wind fields. The wind field model can be used for quality control of the unique wind estimate from point-wise ambiguity removal algorithms. In objective ambiguity removal algorithms [*Schroeder et al.*, 1985; *Shaffer et al.*,

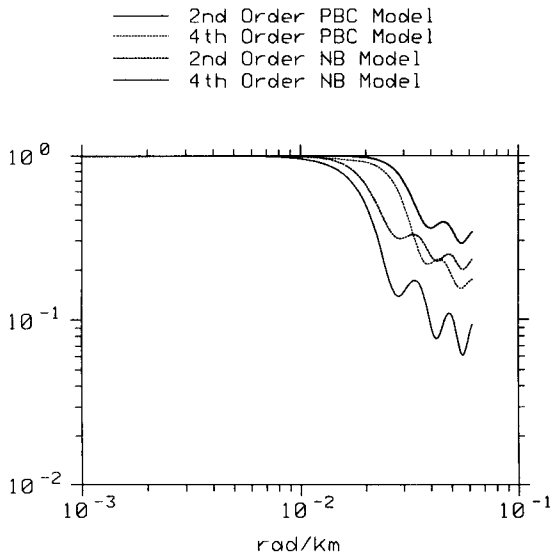

Fig. 2. Slices of the model magnitude wavenumber response for various model options along the line $k_x = 0$ and $k_y \geq 0$. The model size is $M = N = 10$ and $N_p = 10$.

1991], ambiguity selection errors often occur in spatially correlated groups or "clumps" and result in unrealistic wind field estimates. Such errors can be detected by fitting the wind field model to the unique wind field and computing the rms error using (21). If the rms direction error is less than a threshold (typically 15°–20°), the wind field may be considered "feasible." However, if the rms direction error is greater than this threshold, it is likely that significant ambiguity selection errors have occurred in the region. In applying (21) in this manner, it is first necessary to fill in missing wind measurements in the point-wise wind field estimate with an average of the nearby measurements.

5. SIMULATION STUDIES

To evaluate the performance of model-based wind estimation for SASS, both simulated and actual SASS measurements have been used. The advantage of simulation is that the actual true wind field is known, permitting detailed performance evaluation. To make the simulation as realistic as possible, the actual SASS measurement geometry and the corresponding actual α, β, and γ parameters in the noise variance equation (equation (14)) were used.

Lacking sufficiently high-resolution wind field data to act as input for the simulation, simulated wind fields were generated from 1.875° resolution European Centre for Medium-Range Weather Forecasts (ECMWF) data interpolated to 10-km resolution with nondivergent small-scale variability added. The added small-scale variability had a spectrum of ak^{-2} [see *Freilich and Chelton*, 1986]. For a given 2000 × 2000 km region the value of a was selected to be consistent with the ECMWF wind field spectrum. Seven fields were selected to span a wide range of meteorological conditions, including sharp fronts and small-scale cyclones from the set used by *Shaffer et al.* [1991].

Five "template" SASS revs covering the Pacific basin were randomly selected. Simulated SASS revs were then generated by "flying" each of the template revs over each of the input wind fields. For a given wind field and template rev, several simulated revs were generated using different realizations of the Monte Carlo noise added to the simulated σ^0 measurements. In generating the simulated revs from the template revs, the actual SASS σ^0 measurements were replaced with the value of σ^0 computed from the observation geometry and the input wind field using the Wentz model function [*Wentz et al.*, 1984]. The corresponding actual SASS α, β, and γ parameters were then used to generate Monte Carlo noise which was added to the computed σ^0 values to simulate the scatterometer measurements. No explicit attitude or geophysical model errors were added. The resulting simulated measurements exhibit the same spatial sampling characteristics (including missing measurements), signal-dependent measurement noise, and measurement geometry as the original SASS measurements but with a known "true" wind field. Each simulated SASS rev was processed using point-wise wind retrieval and model-based wind retrieval. For the point-wise case the ambiguity closest to the true wind was selected as the "ideal unique wind field." Model orders of 2 and 4 were considered for the PBC model with $N_p = 10$. To compute the model-based wind field estimate, both FIT and MINIT initial value computation methods were considered.

A visual illustration of point-wise and model-based wind field estimation is given in Figure 3. In this and the remaining figures, wind vectors are plotted on a 50-km resolution instrument-based cross-track/along-track grid coordinate system. Wind speeds have been plotted so as to enhance the visibility of the wind direction for low wind speeds. The true simulated wind field sampled at the 50-km grid centers is shown in Figure 3*a*. It contains two fronts, one in the left (upper) swath centered at along-track index 221 and a synthetic "front" across both swaths at along-track index 240. The model-based estimate (second-order PBC model with $N_p = 10$ using the FIT initial value computation method) obtained from the simulated σ^0 measurements is shown in Figure 3*b*. The ideal unique wind from the point-wise ambiguity set is shown in Figure 3*c*. The missing wind measurements in Figure 3*c* result from missing σ^0 measurements due to antenna coregistration problems and instrument calibration cycles. While precisely the same σ^0 measurements were used to generate Figure 3*b*, the model-based wind retrieval approach is able to provide wind estimates at each point of the swath. Comparison of the model-based and point-wise wind field estimates in these figures reveals that the model-based wind field estimates (1) are visually less "noisy" and (2) have significantly fewer missing measurements and a wider effective swath. While both fronts in this example are smoothed in the model-based estimate, they remain correctly located and oriented.

5.1. *MINIT Versus FIT*

Thirty-five simulated passes were processed using both the FIT and the MINIT initial value computation methods. In general, both methods produced similar results over the 1995 region locations compared. Some infrequent exceptions, consisting of 10 × 10 regions in which the two estimates did not agree, resulted when the optimization stopped at different local minima. The exceptions could be grouped into three classes. For class one cases the two methods' results differed significantly, but the MINIT solution appeared to be a better estimate of the true wind field than the FIT result. This result was quite rare, occurring only 3 times in the entire simulated data set. For class two cases the FIT-based estimate was a good estimate of the true field, while the MINIT model-based wind estimate appeared unrealistic. For this class the failure of MINIT to find the "correct" solution could be attributed to the failure of the optimization algorithm to locate one or more of the global minima. The particular global minimum of the objective function corresponding to the FIT-based estimate was among those missed. This problem was observed 18 times or just less than 1% of the regions. In the third class both model-based estimates differed significantly from the true wind field (though they may or may not have agreed with each other). Cases in this class could be attributed to the modeling limitations inherent in the second-order model used. Such cases can be detected by examining the rms error resulting from fitting the second-order model to the true wind field, with a large model fit error indicating the inability of the second-order model to adequately model the underlying wind field. Many of the class three errors were associated with the artificial "fronts" in the true wind field. Seven class three errors were identified.

In 11 (~0.5%) of the regions examined, the outer edge (last wind vector estimate which extends 100 km beyond the

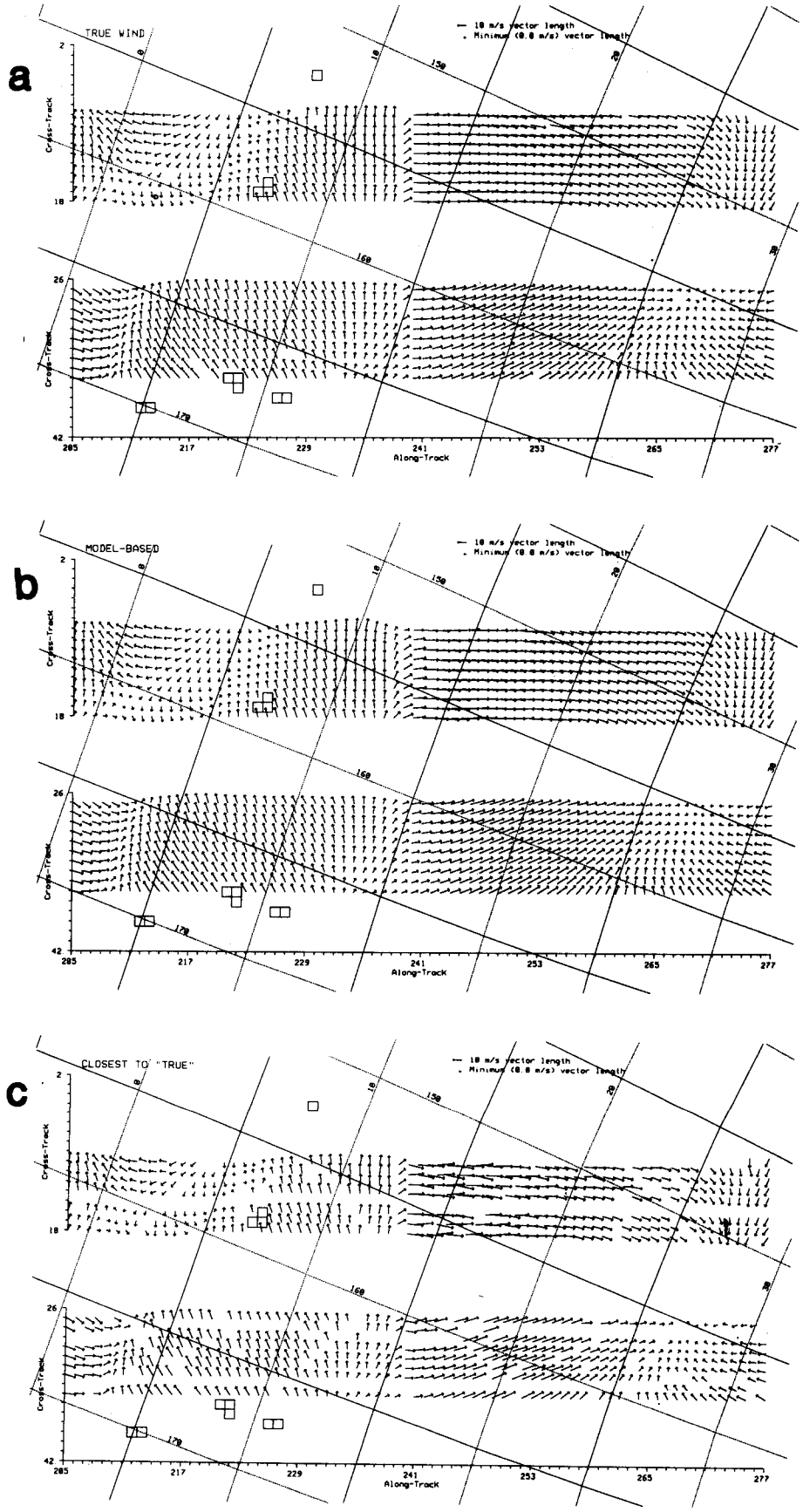

Fig. 3. Simulation example. (*a*) True wind field. (*b*) Model-based estimate second-order PBC model with $N_p = 10$ and $M = N = 10$) from simulated σ^0 measurements of Figure 3*a*. (*c*) Ideal unique point-wise wind field estimate generated from the same simulated σ^0 measurements. The point-wise ambiguity closest to the true wind vector is shown. This represents ideal ambiguity removal. In these and later plots, a vector is shown at each grid point of a 50 $\times$ 50 km grid for which wind estimates can be made using model-based estimation. Squares indicate σ^0 measurements at grid elements containing land. Winds are plotted in the meteorological convention relative to north.

point-wise estimate) of both model-based estimates was observed to have a directional "ripple" error artifact resulting from the lack of sufficient σ^0 measurements in the outer swath region. A typical example of the error is illustrated in example 1 below. This artifact does not occur when there are sufficient azimuth angle observations of σ^0 at the swath edges. This error is the limiting factor in the swath width extension possible with the model-based approach. When the σ^0 measurement coverage over the region is insufficient (e.g., for regions containing more than 25–35% land or at the very start or end of a swath), the model-based estimates can not be expected to perform well and were not included in the visual analysis.

Since both initial value computation methods produced similar results, the FIT initial value computation method with the initial value computed from the point-wise unique wind field was selected as the primary method of processing actual and simulated SASS data.

5.2. *Model Order Selection Revisited*

As previously indicated, selection of the wind field model order requires a trade-off between the accuracy of the wind field model and the computation required to optimize the ML objective function. In addition, the order of the model may affect the number of elements in D_f^c.

To evaluate the effects of the vorticity and divergence field model orders on wind retrieval accuracy, the simulated σ^0 measurements were processed using both second- and fourth-order PBC models. The rms estimate errors were computed and binned by true wind speed. The results are summarized in Table 1 and contrasted with the errors for point-wise wind estimation with ideal ambiguity removal. In Table 1 the vector error is defined as the rms of the vector magnitude of the difference between the true wind vector and the estimated wind vector. Several observations can be made from Table 1. At low wind speeds (<8 m/s) the model-based results for both model orders have lower rms speed, direction, and vector errors than the point-wise estimates, while at higher wind speeds the model order is a factor. For example, the fourth-order model has somewhat better rms direction error than the point-wise estimate which is somewhat better than the second-order model. For wind speeds >8 m/s, point-wise retrieval has somewhat better rms wind speed error than either model-based result. In general, however, the performances of the model-based and point-wise retrievals are similar. For later comparison, the mean and rms differences between the second-order model-based and point-wise wind estimates are given in Table 2.

TABLE 1. Summary of rms Estimate Error for the Simulations Described in the Text

	Wind Speed Range, m/s				
	2–4	4–8	8–12	12–20	20+
Model-based (second order)					
rms direction error deg	11.93	7.65	5.22	5.35	4.13
rms speed error, %	15.1	8.5	5.9	4.6	3.5
rms vector error, %	24.8	15.2	10.6	10.2	7.9
Model-based (fourth order)					
rms direction error deg	11.7	6.95	4.57	3.29	2.70
rms speed error, %	17.7	10.2	6.8	4.9	3.8
rms vector error, %	26.3	15.4	10.1	7.5	6.0
Ideal unique point-wise					
rms direction error deg	15.7	8.51	4.95	4.19	3.83
rms speed error, %	26.2	11.3	4.9	2.0	1.4
rms, vector error, %	38.8	18.9	10.0	7.6	6.8

TABLE 2. Summary Statistics of the Difference Between the Second-Order Model and the Point-Wise Wind Fields With Ideal Ambiguity Removal Estimated From Simulated Data as Described in the Text

	Wind Speed Range, m/s				
	2–4	4–8	8–12	12–20	20+
Number of measurements, %	17	38	23	20	2
Mean direction difference, deg	−0.2	−0.1	0.1	0.1	0.1
Mean speed difference, m/s	−0.03	0.00	0.01	0.03	0.05
rms direction difference, deg	19.1	10.6	6.3	5.5	3.9
rms speed difference, m/s	0.56	0.55	0.60	0.70	0.77
rms vector difference, m/s	1.09	1.16	1.22	1.62	1.64

As an aside, when comparing the performance difference between the models, note that the SNR of the σ^0 measurements is wind speed-dependent, with the SNR much lower at low wind speeds than at high wind speeds. For model-based wind retrieval the modeling error dominates at high wind speeds, while at lower wind speeds the retrieval error is dominated by the σ^0 measurement noise. Thus the performance of both models is comparable at low wind speeds, while a larger model order results in improved accuracy at high wind speeds.

In a visual comparison the second-order model exhibited somewhat more smoothing of frontal features than did the fourth-order model. However, subjectively significant differences were noted in only 19 (~1%) cases. Of these, 13 were associated with artificial "fronts" such as the one illustrated in Figure 3. The remaining six occurred at other fronts or were associated with cyclones. Because the wind estimate accuracy of the second-order and fourth-order models is comparable, a second-order model was used for processing actual SASS data in order to minimize computation.

6. SASS DATA

When using actual SASS measurements, the performance of model-based retrieval is difficult to independently establish, since the ground truth wind field is unknown. While limited ground truth is available, it is geographically sparse and therefore has limited utility in verifying the performance of the model-based wind retrieval scheme. Instead, we must resort to using SASS wind estimates made by point-wise wind retrieval. Ambiguity selection errors in the point-wise wind estimates, plus the noise levels in the point-wise retrieved winds, complicate the use of these wind estimates for comparison with the model-based winds.

While unique SASS wind data sets have been generated using objective ambiguity removal [e.g., *Atlas et al.*, 1987], on close inspection these were found to contain numerous localized regions of ambiguity selection errors with sharp, artificial boundaries surrounding the regions. Instead, the *Wurtele et al.* [1982] subjective ambiguity removal data set was used to generate reference wind fields. The Wurtele data set consists of 9 days of SASS winds retrieved on a 100-km grid using the SASS1 model function [*Bracalente et al.*, 1980] with subjective ambiguity removal using available auxiliary meteorological data. A detailed analysis of this data

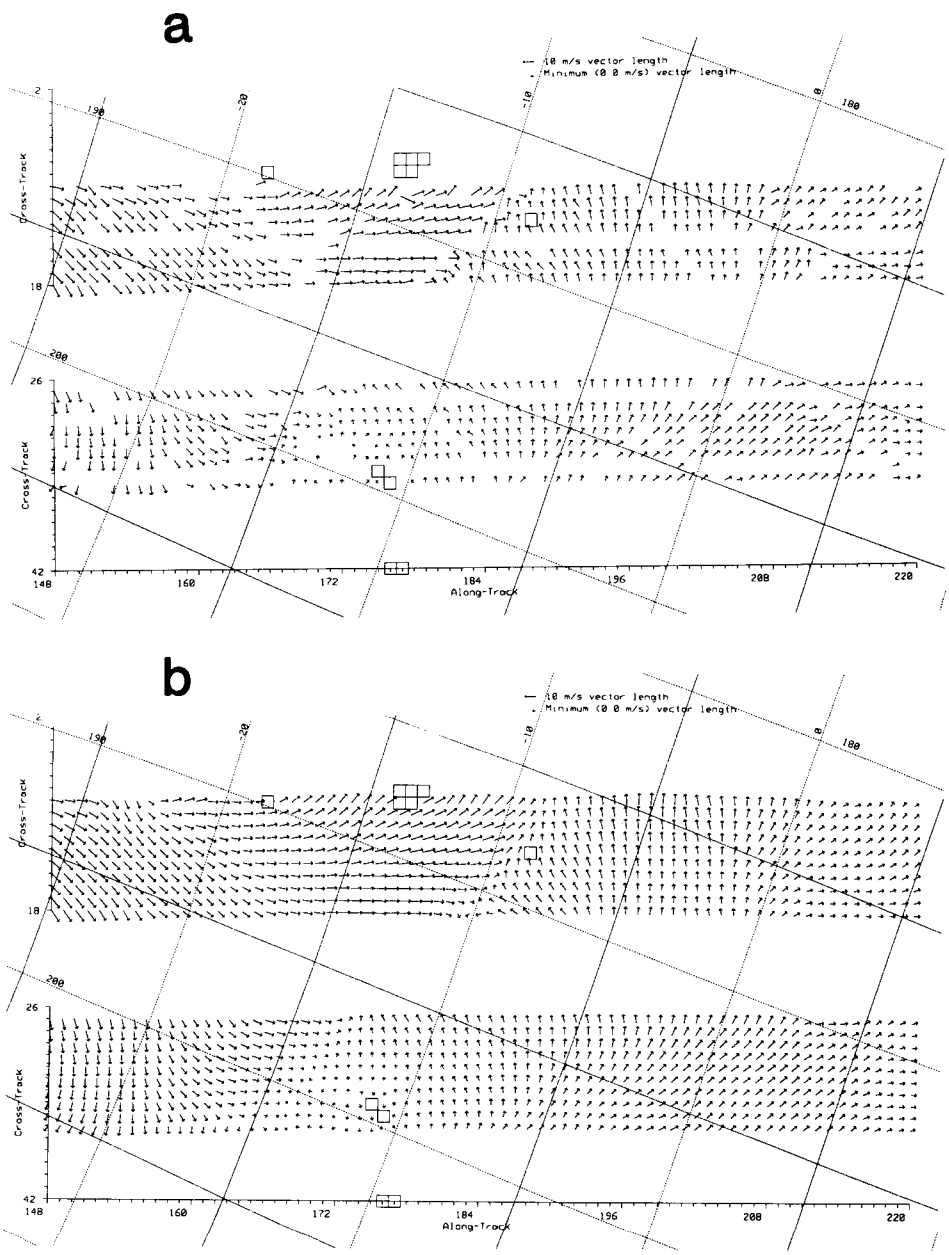

Fig. 4. Actual SASS measurement example for Seasat rev 1070, September 9, 1978. (*a*) Point-wise reference subjective ambiguity removal data set. (*b*) Model-based estimate using a second-order PBC model with $N_p = 10$ and a region size of $M = 10 \times N = 10$ with 50% overlap.

set and comparison with the Atlas data set is given by *Chelton et al.* [1989].

Since 50-km resolution winds were needed to compare with the model-based wind estimates, a "reference data set" was first generated by using point-wise estimation of the SASS winds on a 50-km grid using the Wentz model function [*Wentz et al.*, 1984]. The ambiguity closest to the corresponding Wurtele unique wind direction was then selected. Note that the Wurtele result is based on many man-hours of expert ambiguity removal.

6.1. *Case Studies*

A detailed visual comparison of the model-based winds and the point-wise reference set was conducted using 28 revs. In general, the model-based winds and reference sets exhibited good general agreement, though some apparent smoothing of fronts in the model-based results was noted (see example 1). The model-based wind fields contained approximately 30% more wind vectors than did the reference set. Small direction and speed differences between the two estimates were common (see the examples below). Such differences are attributed to noise in the point-wise estimates, possible point-wise ambiguity selection errors, and/or smoothing in the model-based estimates. It was noted that the point-wise reference set appeared to have significantly more directional "noise" than the point-wise simulation results (e.g., see Figures 3 and 4).

In approximately 1.5% of the regions examined, a subjectively significant difference between the model-based and reference winds was noted. In approximately one half of

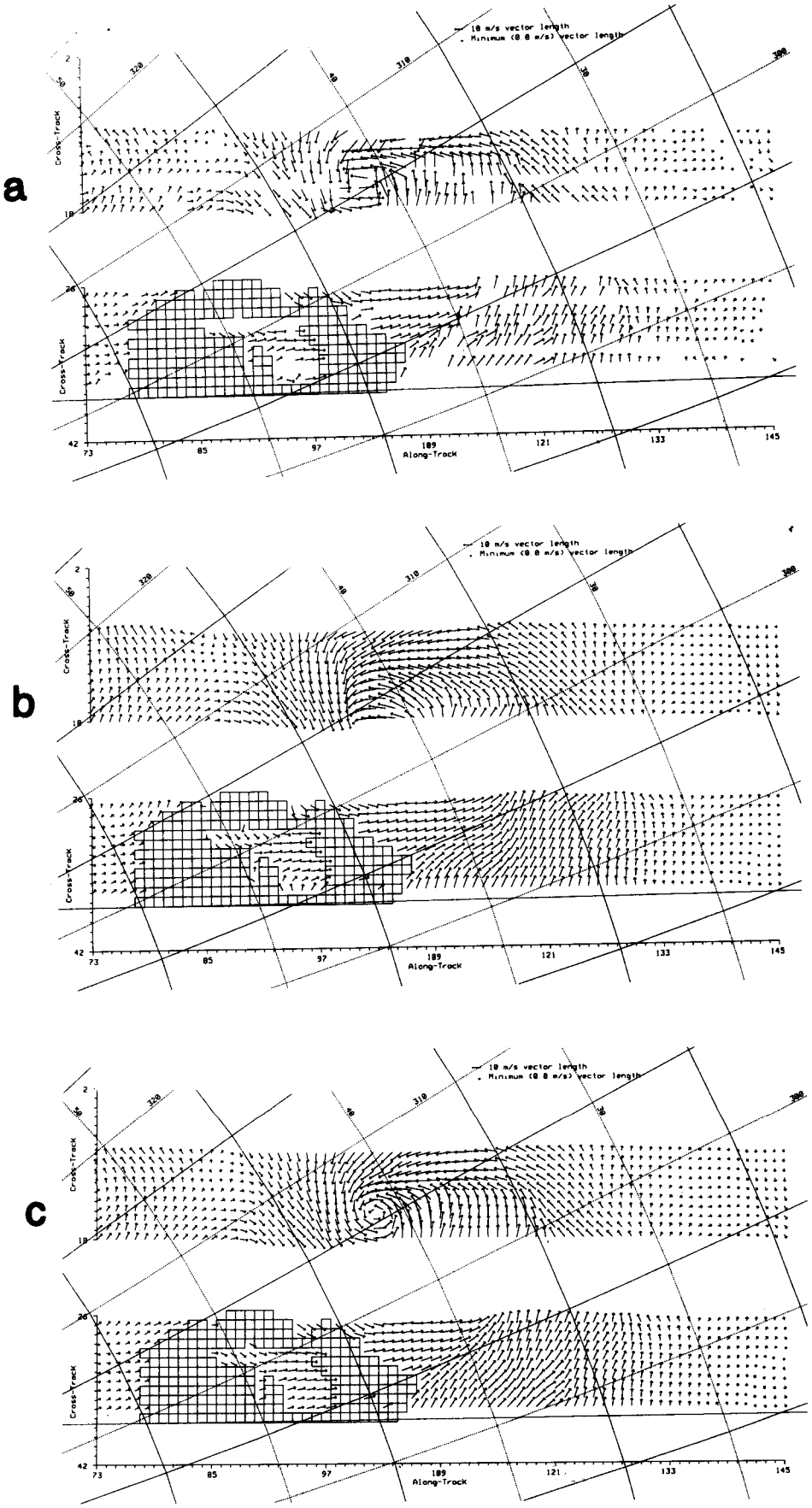

Fig. 5. Actual SASS measurement example for Seasat rev 1075, September 10, 1978. The center of the QE-II storm is near the center of the left (upper) swath. (*a*) Point-wise reference subjective ambiguity removal data set. (*b*) Model-based (second-order model) estimate. Note the incorrect location of the storm center due to the limited capability second-order model used. (*c*) Model-based (fourth-order model) estimate. The fourth-order model is able to adequately model the very tight storm, resulting in a successful wind field estimate.

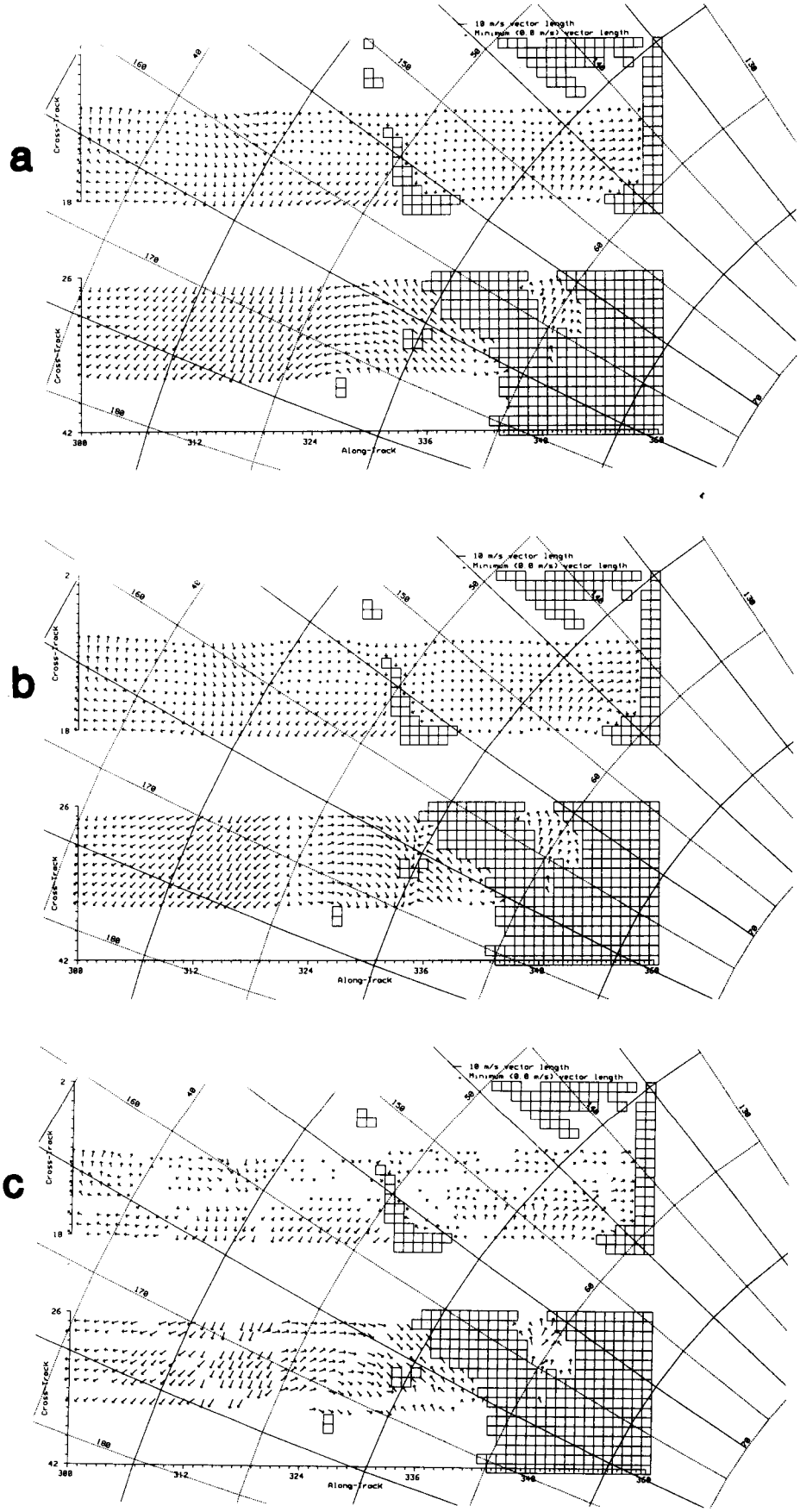

Fig. 6. Actual SASS measurement example for Seasat rev 1071, September 9, 1978. (*a*) Model-based (second-order model) estimate based on the MINIT initial value computation method. MINIT has resulted in a well-defined, realistic wind field over the region. (*b*) Model-based (second-order model) estimate based on the FIT initial value computation method (see text). (*c*) Point-wise reference subjective ambiguity removal data set. Note that the ambiguity selected for the region to the left of the land on the lower (right) swath is in error by ~180°.

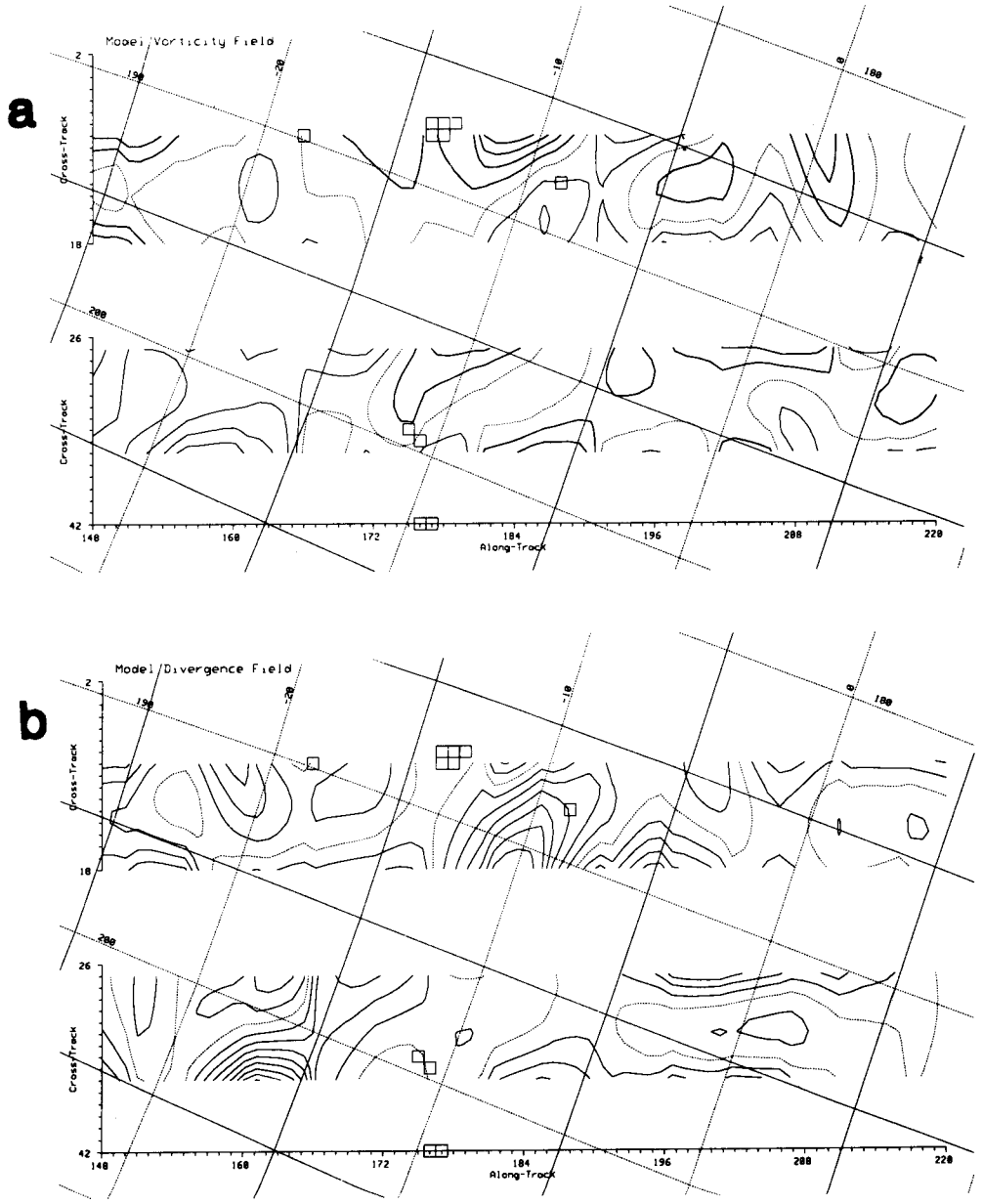

Fig. 7. (*a*) Vorticity and (*b*) divergence field estimates derived from the wind field parameters estimated for Figure 4. The contour intervals are arbitrary: thick lines correspond to positive, dotted line corresponds to zero, and thin lines correspond to negative.

these cases, the difference was apparently due to a problem in the model-based estimate such as an inadequate model order or the failure of the optimization. For the remaining cases the reference set did not appear realistic because of possible ambiguity removal errors (example 3 contains a dramatic example). In less than 3% of the regions examined, the outer edge (last wind vector estimate) of the model-based estimate (which extends 100 km beyond the point-wise estimate) was observed to have a directional "ripple" error artifact (illustrated in example 1) resulting from the lack of sufficient σ^0 measurements in the outer swath region. The larger percentage of edge artifacts in the actual data may be due in part to geophysical modeling errors.

The following sections present three visual examples comparing the model-based and subjective point-wise estimated winds. These were selected to illustrate the strengths and weaknesses of model-based wind retrieval. The general agreement of the model-based winds and the Wurtele winds leads to the conclusion that the Wurtele ambiguity selection is usually very good.

6.1.1. *Example 1: Pacific Basin.* A visual comparison of model-based and point-wise wind retrieval for actual SASS data (a portion of Seasat rev 1070, September 9, 1978) may be made (Figure 4). The point-wise reference wind field based on subjective ambiguity removal is illustrated in Figure 4*a* with the corresponding model-based wind field shown in Figure 4*b*. As in previous figures, a scatterometer-based coordinate system with positions specified in terms of along-track and cross-track distance is used. A minimum length vector is used for low wind speeds in order to highlight the wind direction.

Comparing Figures 4*a* and 4*b*, we note that the model-

based estimate swath (1) is wider and (2) has fewer missing wind measurements. (The missing wind measurements arise in point-wise wind retrieval when there are not enough azimuthal σ^0 measurements to retrieve the wind or when the wind speed drops below 2 m/s where the geophysical model function is not well defined.) In contrast, the model-based wind field estimate has a uniform swath width without missing measurements. It should be noted that many of the σ^0 sampling problems encountered with SASS measurements will not occur for ERS 1 and NSCAT.

In this example a front (centered at approximately along-track index 180) extends diagonally across the left (upper) swath. Along this front the point-wise winds exhibit some confusion due to errors in the ambiguity removal and the inherent σ^0 measurement under sampling. While the model-based retrieval has smoothed the sharp change in the wind field along the front, its location is unchanged. A direction "ripple" artifact along the outer swath edge is evident at along-track index 150 on the left (upper) swath.

6.1.2. *Example 2: QE-II storm.* The explosive QE-II storm of 1978 was not well forecast with the tools of the era and has become a "classic" case to support space-based remote sensing. The left SASS wind vector swath passed directly over the storm center east of Newfoundland on September 10, 1978, on rev 1075 at approximately 0245 UT. The point-wise reference wind field based on subjective ambiguity removal for this pass is illustrated in Figure 5*a*. Unfortunately, the very tight structure of this particular storm could not be adequately modeled by the second-order PBC model. As a result, the second-order model-based estimate failed to correctly locate the storm center (see Figure 5*b*) resulting in an error. However, the fourth-order PBC model, with its improved modeling capability, accurately modeled the storm circulation pattern. The fourth-order model-based estimate is shown in Figure 5*c*.

In an experiment to compare the performance of the second- and fourth-order models with actual data, 11 revs were processed using FIT for both second- and fourth-order models. These were compared with the subjective reference set. As in the simulations, there was generally good agreement between the model orders with the second-order model exhibiting somewhat more smoothing than the fourth-order model. The cases for which there were subjectively significant differences could be grouped into four classes. In the first class the second-order model appeared to be unable to adequately model the actual wind field, while the fourth-order model performed well; that is, there was good agreement between the fourth-order model result and the point-wise reference set. Most examples of this class were tight cyclonic wind patterns or very sharp fronts (e.g., Figure 5). Of the 11 revs (containing approximately 1265 regions) examined, this class was observed 9 times. In class two the second-order model appeared to be in better agreement with the reference set than the fourth-order model. Only one case of this class was observed. For class three, possible ambiguity selection errors and/or missing measurements in the reference set made it impossible to select between the model orders. Eight examples of this class were identified. In the fourth class the model-based estimates generally followed the subjective set which appeared unrealistic. Three cases from this class were observed. The small total percentage (~1.6%) of exceptions observed supports the decision to use the second-order model to process the complete data set.

6.1.3. *Example 3: North Pacific.* The final example illustrates a case from rev 1071, September 9, 1978, in which the model-based wind estimate generated using MINIT (shown in Figure 6*a*) differs significantly from the estimate generated by FIT because of ambiguity selection errors in the reference data set. As is readily apparent in Figure 6*c*, which shows the reference subjective ambiguity selection data, the reference data set has a region of significant ambiguity selection errors in the right (lower) swath just to the south of the Kamchatka coast. In this region the vectors should be reversed ~180° in order to produce a more realistic wind field in the northern Pacific. The model-based estimate generated via the FIT method (shown in Figure 6*b*) exhibits unrealistic behavior over the boundaries of the subjective ambiguity selection error region. Over these boundaries the objective function optimization stopped at a local minimum in the objective function. However, the model-based estimate generated via MINIT correctly estimated this wind field.

This problem in the FIT method can be detected by monitoring the rms change between the initial value and the optimized estimate. When the change is large, the FIT-based estimate accuracy is suspect, and the more sophisticated (and time consuming) MINIT method should be used instead. Thus the model-based estimation procedure can be used to detect and correct at least some ambiguity selection errors in the point-wise data set.

As a check, 10 revs were processed using both FIT and MINIT, and the results were compared with the reference set. As predicted by the simulation results, there was good agreement between the results. Four classes of exceptions were noted. For cases in class one it was possible to verify the existence of errors in the ambiguity selection in the subjective reference field with the model-based wind estimate appearing "correct" (e.g., Figure 6). In class two both model-based estimates and the reference wind fields appeared realistic, but because of the lack of collaborative data it was impossible to evaluate the "correctness" of either result. For class three the MINIT model-based wind estimate appeared unrealistic, while the FIT-based estimate and the subjective reference set appeared realistic and were in general agreement. In this case the MINIT was considered to have failed to find the "correct" solution because of the failure of the optimization algorithm to locate all the global minima of the objective function. No particular meteorological conditions were associated with these failures. For the fourth class the point-wise estimate appeared realistic, but both model-based estimates failed to represent the key features of the point-wise field or appeared unrealistic. This was attributed to the modeling limitation of the second model order used (see example 2) and/or failure of the optimization algorithm. Of the 10 revs (containing approximately 1140 regions) examined, class one was observed once; class two, 5 times; class three, once, and class four, 3 times. Because these exceptions constituted only a small percentage (~1%) of the total regions processed, the decision to use the FIT initial value computation method to process the full data set is justified. We note that when applying the method to other scatterometers, the FIT initial value computation method can only be used if a sufficiently high-quality reference field is available. Otherwise, the MINIT method must be used.

TABLE 3. Summary Global Statistics of the Model-Based Minus the Point-Wise Wind Estimates for Actual SASS Data

	Wind Speed Range, m/s				
	2–4	4–8	8–12	12–20	20+
Global ocean 60°S to 60°N					
Number of measurements, %	16	40	29	14	0.5
Mean direction difference, deg	−0.5	−0.2	−0.1	−0.1	−0.4
Mean speed difference, m/s	−0.21	−0.18	−0.15	−0.12	0.23
rms direction difference, deg	32.8	20.9	16.8	15.4	18.3
rms speed difference, m/s	1.03	0.96	0.99	1.08	1.60
rms vector difference, m/s	1.94	2.26	2.85	3.83	6.73
Northern hemisphere 0° to 60°N					
Number of measurements, %	23	48	22	7	0.3
Mean direction difference, deg	−0.3	−0.3	0.0	−0.3	−6.0
Mean speed difference, m/s	−0.18	−0.16	−0.15	−0.09	0.00
rms direction difference, deg	32.4	21.0	16.3	16.3	23.0
rms speed difference, m/s	0.85	0.89	0.92	1.01	1.26
rms vector difference, m/s	1.78	2.17	2.72	4.00	9.38
Southern hemisphere 60°S to 0°					
Number of Measurements, %	12	36	50	19	0.6
Mean direction difference, deg	−0.6	−0.1	−0.1	−0.1	1.4
Mean speed difference, m/s	−0.24	−0.19	−0.15	−0.13	0.30
rms direction difference, deg	33.2	20.8	17.0	15.3	15.2
rms speed difference, m/s	1.20	1.01	1.01	1.10	1.70
rms vector difference, m/s	2.10	2.33	2.90	3.80	5.57

TABLE 4. Summary Statistics for the Atlantic Ocean of the Model-Based Minus the Point-Wise Wind Estimates for Actual SASS Data

	Wind Speed Range, m/s				
	2–4	4–8	8–12	12–20	20+
Atlantic Ocean 60°S to 40°S					
Number of measurements, %	11	25	26	36	2
Mean direction difference, deg	−1.5	−0.2	0.5	0.7	−0.8
Mean speed difference, m/s	−0.53	−0.48	−0.45	−0.30	−0.12
rms direction difference, deg	45.6	32.0	27.5	20.9	21.9
rms speed difference, m/s	2.10	1.82	2.01	1.63	2.38
rms vector difference, m/s	3.22	3.85	5.07	5.30	8.00
Atlantic Ocean 40°S to 20°S					
Number of measurements, %	17	32	32	18	0.6
Mean direction difference, deg	−0.1	0.6	0.1	−0.9	3.3
Mean speed difference, m/s	−0.17	−0.15	−0.14	−0.05	0.31
rms direction difference, deg	25.8	17.7	15.4	12.9	14.1
rms speed difference, m/s	0.86	0.87	0.84	0.84	0.98
rms vector difference, m/s	1.57	1.97	2.63	3.23	5.33
Atlantic Ocean 20°S to 0°					
Number of measurements, %	14	63	22	0.3	0
Mean direction difference, deg	0.9	−0.4	−0.2	4.3	N/A
Mean speed difference, m/s	−0.05	−0.07	−0.03	−0.60	N/A
rms direction difference, deg	16.9	11.2	7.8	20.5	N/A
rms speed difference, m/s	0.52	0.55	0.49	2.58	N/A
rms vector difference m/s	1.03	1.30	1.34	5.66	N/A
Atlantic Ocean 0° to 20°N					
Number of measurements, %	24	60	16	0.2	0
Mean direction difference, deg	1.7	0.5	−0.7	−3.4	N/A
Mean speed difference, m/s	−0.10	−0.09	−0.03	0.09	N/A
rms direction difference, deg	23.7	13.7	10.6	5.3	N/A
rms speed difference, m/s	0.63	0.68	0.57	0.81	N/A
rms vector difference, m/s	1.35	1.50	1.69	1.43	N/A
Atlantic Ocean 20°N to 40°N					
Number of measurements, %	20	49	24	6	0.3
Mean direction difference, deg	−0.2	−0.7	1.0	0.0	−4.8
Mean speed difference, m/s	−0.20	−0.17	−0.15	−0.21	−0.25
rms direction difference, deg	30.9	19.8	17.0	27.9	29.1
rms speed difference, m/s	0.87	0.84	0.97	1.38	1.52
rms vector difference, m/s	1.77	2.13	2.84	6.64	10.61
Atlantic Ocean 40°N to 60°N					
Number of measuremetns, %	8	27	30	31	3
Mean direction difference, deg	−3.3	−3.0	−0.5	−0.6	−6.2
Mean speed difference, m/s	−0.25	−0.31	−0.27	−0.11	0.02
rms direction difference, deg	45.2	33.4	18.9	15.0	25.3
rms speed difference, m/s	1.01	1.15	1.04	0.95	1.24
rms vector difference, m/s	2.34	3.34	3.24	3.84	9.32

TABLE 5. Summary Statistics for the Indian Ocean of the Model-Based Minus the Point-Wise Wind Estimates for Actual SASS Data

	Wind Speed Range, m/s				
	2–4	4–8	8–12	12–20	20+
Indian Ocean 60°S to 40°S					
Number of measurements, %	4	17	34	44	2
Mean direction difference, deg	0.8	−0.1	−0.4	0.3	3.1
Mean speed difference, m/s	−1.18	−0.57	−0.33	−0.15	0.37
rms direction difference, deg	52.2	32.6	25.1	15.9	10.6
rms speed difference, m/s	3.35	1.86	1.38	1.06	1.31
rms vector difference, m/s	4.74	3.96	4.14	3.93	4.08
Indian Ocean 40°S to 20°S					
Number of measurements, %	16	39	33	12	0.1
Mean direction difference, deg	2.9	−1.3	−0.7	−0.1	2.7
Mean speed difference, m/s	−0.22	−0.19	−0.13	−0.07	0.08
rms direction difference, deg	31.8	21.7	16.2	10.2	4.4
rms speed difference, m/s	0.98	0.94	0.86	0.89	0.65
rms vector difference, m/s	1.90	2.29	2.60	2.51	1.77
Indian Ocean 20°S to 0°					
Number of measurements, %	17	41	36	6	0
Mean direction difference, deg	−2.1	0.0	0.0	0.2	N/A
Mean speed difference, m/s	−0.14	−0.12	−0.05	0.0	N/A
rms direction difference, deg	32.1	16.8	10.8	8.5	N/A
rms speed difference, m/s	0.88	0.81	0.66	0.70	N/A
rms vector difference, m/s	1.75	1.81	1.84	1.96	N/A
Indian Ocean 0° to 20°N					
Number of measuremetns, %	27	53	20	0.5	0
Mean direction difference, deg	0.4	0.4	0.1	−2.5	N/A
Mean speed difference, m/s	−0.16	−0.16	−0.10	0.36	N/A
rms direction difference, deg	27.3	18.3	14.5	8.9	N/A
rms speed difference, m/s	0.80	0.87	0.94	1.00	N/A
rms vector difference, m/s	1.60	1.96	2.45	2.12	N/A

6.2. *Vorticity and Divergence Fields*

As part of the estimation of the wind field, the model-based wind estimation approach described in this paper also determines the wind field vorticity and divergence via the models for these scalar fields. Given the wind field model parameter vector estimated from the σ^0 measurements, the vorticity and divergence fields can be computed. Since these auxiliary product fields are, in effect, estimated directly from the σ^0 measurements, they are much less noisy than estimates computed by differencing conventional point-wise winds. Furthermore, the estimated fields are available at the full width of the wind vector swath and have fewer "holes." Illustrations of the model-based estimates of the wind vorticity and divergence fields (corresponding to the model-based wind field estimate in Figure 4*b*) are given in Figure 7. In Figure 7 the contour levels are arbitrary. An extensive study of the vorticity and divergence of SASS winds is underway and will be reported in a future paper.

7. SASS DATA: OVERALL STATISTICS

The FIT initial value computation technique and a second-order model were used to process 9 days (Seasat rev 1016, September 6, 1978, through rev 1144, September 15, 1978) of SASS data corresponding to the Wurtele data set. After processing, a detailed comparison of the model-based and point-wise reference set (which is based on the ambiguity removal of the Wurtele data set) was made. A statistical summary of the difference between the model-based wind estimate and the point-wise reference set that is broken down by geographical region is given in Tables 3–6. In Tables 3–6 the statistics were binned according to the model-based wind speed. The errors in Tables 3–6 may be compared with the simulation results in Table 2. Note, however, that the simulation results in Table 2 are based on ideal ambiguity removal, while the reference set used to compute Tables 3–6 contains ambiguity selection errors. In general, the rms and mean differences are larger for actual data than predicted from the simulations. Since the true, underlying wind field is not known, it is difficult to be quantitative in evaluating the overall measurement accuracy [cf. *Chelton et al.*, 1989].

Table 3 provides a summary of the differences between point-wise and model-based results. From Table 3 we conclude that there is only a limited difference in performance in the northern and southern hemispheres. The model-based wind speed estimates are biased slightly lower than the point-wise estimates with a smaller bias at higher wind speeds. The mean wind direction difference is essentially zero. The rms wind direction difference is reduced at higher wind speeds. The higher rms wind direction difference at low wind speeds may be the result of the high directional "noise" and ambiguity selection errors in the point-wise estimates at low wind speeds. Globally, the rms speed difference is approximately 1 m/s, well below the stated 2 m/s accuracy of the scatterometer system [*Jones et al.*, 1982].

From Tables 4–6 we note some variations in the differences for latitude bands, though there is general similarity between ocean basins. At high latitudes (60°S to 40°S and 40°N to 60°N) the rms errors are significantly larger than for low-latitude bands. This may be due to the higher variability of the wind in these regions. However, the number of ambiguity selection errors also appeared to be largest in

TABLE 6. Summary Statistics for the Pacific Ocean of the Model-Based Minus the Point-Wise Wind Estimates for Actual SASS Data

	Wind Speed Range, m/s				
	2–4	4–8	8–12	12–20	20+
Pacific Ocean 60°S to 40°S					
Number of measurements, %	4	20	34	41	2
Mean direction difference, deg	−0.8	0.2	0.5	0.6	1.4
Mean speed difference, m/s	−1.07	−0.57	−0.30	−0.18	0.27
rms direction difference, deg	51.8	33.5	25.1	17.1	12.9
rms speed difference, m/s	2.88	1.88	1.40	1.24	1.60
rms vector difference, m/s	4.30	4.06	4.16	4.20	5.0
Pacific Ocean 40°S to 20°S					
Number of measurements, %	16	38	33	14	0.2
Mean direction difference, deg	−1.6	−1.0	−0.4	−0.3	−0.8
Mean speed difference, m/s	−0.21	−0.19	−0.12	−0.09	0.1
rms direction difference, deg	31.3	21.2	16.1	10.9	8.0
rms speed difference, m/s	0.95	0.94	0.84	0.92	0.83
rms vector difference, m/s	1.85	2.24	2.59	2.76	2.99
Pacific Ocean 20°S to 0°					
Number of measurements, %	19	42	35	5	0
Mean direction difference, deg	−0.22	−0.1	0.2	0.3	N/A
Mean speed difference, m/s	−0.13	−0.12	−0.06	0.0	N/A
rms direction difference, deg	30.3	17.6	11.3	9.8	N/A
rms speed difference, m/s	0.82	0.84	0.67	0.78	N/A
rms vector difference, m/s	1.66	1.84	1.90	2.20	N/A
Pacific Ocean 0° to 20°N					
Number of measurements, %	27	54	18	0.7	0
Mean direction difference, deg	−0.2	0.5	−0.6	−4.7	N/A
Mean speed difference, m/s	−0.19	−0.16	−0.10	0.38	N/A
rms direction difference, deg	31.3	19.4	16.8	23.0	N/A
rms speed difference, m/s	0.88	0.91	1.17	1.58	N/A
rms vector difference, m/s	1.81	2.07	2.92	4.76	N/A
Pacific Ocean 20°N to 40°N					
Number of measurements, %	32	41	21	6	0
Mean direction difference, deg	3.6	1.3	2.7	4.3	N/A
Mean speed difference, m/s	−0.20	−0.19	−0.130	−0.18	N/A
rms direction difference, deg	32.3	25.3	19.8	19.8	N/A
rms speed difference, m/s	0.87	0.99	1.08	1.07	N/A
rms vector difference, m/s	1.77	2.54	3.53	4.6	N/A
Pacific Ocean 40°N to 60°N					
Number of measurements, %	22	40	19	18	0
Mean direction difference, deg	−4.4	−3.1	−0.3	−1.8	N/A
Mean speed difference, m/s	−0.23	−0.32	−0.42	−0.02	N/A
rms direction difference, deg	47.1	28.7	24.2	14.3	N/A
rms speed difference, m/s	1.06	1.30	1.42	1.26	N/A
rms vector difference, m/s	2.39	3.05	4.30	3.73	N/A

these regions. The differences were smallest near the equator in the Atlantic Ocean.

The lack of sufficient ground truth limits our ability to quantify the accuracy of the model-based wind retrieval technique. However, visual and statistical comparison of model-based wind retrieval with point-wise wind retrieval (and subjective ambiguity removal) suggests that the model-based winds have accuracy comparable to the point-wise winds.

8. Discussion and Conclusions

For traditional point-wise wind retrieval, ambiguity removal is required to select a unique wind direction. Unfortunately, this process is error-prone. Model-based wind retrieval can ameliorate the need for point-wise ambiguity removal. It can also provide more accurate estimates of the wind with fewer "holes" in the wind estimate swath.

Like other model-based methods, development and selection of the model play key roles in the method's performance. However, for model-based wind retrieval a simplified dynamic wind field model provides adequate modeling accuracy for the retrieval of winds from noisy σ^0 measurements. The modeling method presented here provides a trade-off between the model accuracy and the computation required to estimate the wind using the model and permits control of any "smoothing" introduced by the model. The model can also be used as a data quality check for conventional ambiguity selection.

When applied to SASS, which has only two azimuth angles for measuring σ^0, there may be several wind fields which minimize the model-based maximum likelihood objective function used to estimate the wind field model parameters; hence "field-wise" ambiguity removal may be required. While this is conceptually much easier than point-wise ambiguity removal, this step can be avoided if a good initial value can be obtained. Generally, such an initial value can be computed from the point-wise estimate of the wind. This issue is further simplified for three azimuth angle scatterometers such as ERS-1 and NSCAT.

Using model-based wind retrieval, 9 days of SASS data,

for which subjective ambiguity removal of point-wise estimated winds are available, were processed. Careful comparison of the point-wise and model-based results demonstrates the feasibility of the new technique. On the basis of actual data and simulation the accuracy of the wind estimated using model-based retrieval is comparable to the accuracy of the point-wise wind estimates.

Model-based wind field estimation offers several advantages over traditional point-wise wind retrieval: (1) since point-wise ambiguity removal is not required, the problems and issues associated with point-wise ambiguity removal are eliminated, (2) wind measurement accuracy is increased at low wind speeds, (3) there are fewer data gaps, and (4) fuller use of the available σ^0 measurements results in a wider, uniform swath width. Although model-based wind estimation requires more computation than point-wise retrieval, model-based wind estimation has reduced sensitivity to σ^0 measurement noise since it takes advantage of the inherent correlation in the wind field over the measurement swath. Because model-based estimation is more tolerant of noise in the σ^0 measurements than is the point-wise wind estimation technique, its use may permit reductions in the size and weight of future scatterometer instruments by reducing the requirements on the SNR of the σ^0 measurements, permitting smaller transmitters and/or smaller antennas.

Acknowledgments. I would like to thank Michael Freilich for his encouragement and for generating the simulated wind fields. I am pleased to acknowledge the support of NASA Headquarters Physical Oceanography Program directors Gary Lagerloef (through 1990) and David Adamec (current). Part of this research was conducted while the author was at the Jet Propulsion Laboratory, California Institute of Technology.

REFERENCES

Atlas, R., A. J. Busalaci, M. Ghil, S. Bloom, and E. Kalnay, Global surface wind flux fields from model assimilation of Seasat data, *J. Geophys. Res.*, *92*(C6), 6477–6487, 1987.

Bijlsma, S. J., L. M. Hafkenscheid, and P. Lynch, Computation of the stream function and velocity potential and reconstruction of the wind field, *Mon. Weather Rev.*, *114*, 1547–1551, 1986.

Bracalente, E. M., D. H. Boggs, W. L. Grantham, and J. L. Sweet, The SASS scattering coefficient (σ^0) algorithm, *IEEE J. Oceanic Eng.*, *OE-5*(2), 145–153, 1980.

Chelton, D. B., M. H. Freilich, and J. R. Johnson, Evaluation of unambiguous vector winds from the Seasat scatterometer, *J. Atmos. Ocean. Technol.*, *6*, 1024–1039, 1989.

Freilich, M. H., Satellite scatterometer comparisons with surface measurements: Techniques and Seasat results, in Proceedings of a Workshop on ERS-1 Wind and Wave Calibration, 2–6 June 1986, *Eur. Space Agency Spec. Publ., ESA SP-262*, 57–62, 1986.

Freilich, M. H., and D. B. Chelton, Wavenumber spectra of Pacific winds measured by the Seasat scatterometer, *J. Phys. Oceanogr.*, *16*(4), 741–757, 1986.

Grantham, W. L., E. M. Bracalente, C. L. Britt, Jr., F. J. Wentz, W. L. Jongs, Jr., and L. C. Schroeder, Performance evaluation of an operational spaceborne scatterometer, *IEEE Trans. Geosci. Remote Sens.*, *GE-20*(3), 240–254, 1982.

Hoffman, R. N., SASS wind ambiguity removal by direct minimization, *Mon. Weather Rev.*, *110*, 434–445, 1982.

Jones, W. L., L. C. Schroeder, D. H. Boggs, E. M. Bracalente, R. A. Brown, G. J. Dome, W. J. Pierson, and F. J. Wentz, The Seasat-A satellite scatterometer: The geophysical evaluation of remotely sensed wind vectors over the ocean, *J. Geophys. Res.*, *87*(C5), 3297–3317, 1982.

Long, D. G., Model-based estimation of wind fields over the oceans from wind scatterometer measurements, Ph.D. dissertation, Univ. of South. Calif., Los Angeles, Jan. 1989.

Long, D. G., and J. M. Mendel, Model-based estimation of wind fields over the Ocean from scatterometer measurements, I, The wind field model, *IEEE Trans. Geosci. Remote Sens.*, *28*(2), 349–360, 1990*a*.

Long, D. G., and J. M. Mendel, Model-based estimation of wind fields over the ocean from scatterometer measurements, II, Estimation of the model parameters, *IEEE Trans. Geosci. Remote Sens.*, *28*(2), 361–373, 1990*b*.

Long, D. G., and J. M. Mendel, Identifiability in wind estimation from wind scatterometer measurements, *IEEE Trans. Geosci. Remote Sens.*, *29*(2), 268–276, 1991.

Lynch, P., Deducing the wind from vorticity and divergence, *Mon. Weather Rev.*, *116*, 86–93, 1988.

Mendel, J. M., *Discrete Techniques of Parameter Estimation*, Marcel Dekker, New York, 1973.

Naderi, F., M. H. Freilich, and D. G. Long, Spaceborne radar measurement of wind velocity over the ocean—An overview of the NSCAT scatterometer system, *Proc. IEEE*, *79*(6), 850–866, 1991.

Overland, J. E., and J. G. Wilson, Mesoscale variability in marine winds at mid-latitude, *J. Geophys. Res.*, *89*(C6), 10,599–10,614, 1984.

Schroeder, L. C., W. L. Grantham, E. M. Bracalente, C. L. Britt, K. S. Shanmugam, F. J. Wentz, D. P. Wyle, and B. B. Hinton, Removal of ambiguous wind directions for a Ku-band wind scatterometer using measurements at three different azimuth angles, *IEEE Trans. Geosci. Remote Sens.*, *GE-23*(2), 91–100, 1985.

Shaffer, S. J., R. S. Dunbar, V. Hsiao, and D. G. Long, A median-filter-based ambiguity removal algorithm for NSCAT, *IEEE Trans. Geosci. Remote Sens.*, *29*(1), 167–174, 1991.

Ulaby, F. T., R. K. Moore, and A. K. Fung, *Microwave Remote Sensing—Active and Passive*, vol. 1 and 2, Addison-Wesley, Reading, Mass., 1981*a*.

Wentz, F. J., S. Peteherych, and L. A. Thomas, A model function for ocean radar cross-sections at 14.6 GHz, *J. Geophys. Res.*, *89*(C5), 3689–3704, 1984.

Wurtele, M. G., P. M. Woiceshyn, S. Peteherych, M. Borowski, and W. S. Appleby, Wind direction alias removal studies of Seasat scatterometer-derived wind fields, *J. Geophys. Res.*, *87*(C5), 3365–3377, 1982.

Yu, T.-Y., A technique for deducing wind direction from satellite microwave measurements of wind speed, *Mon. Weather Rev.*, *115*, 1929–1939, 1987.

D. G. Long, Electrical and Computer Engineering Department, 459 Clyde Building, Brigham Young University, Provo, UT 84604.

(Received August 25, 1992;
revised March 31, 1993;
accepted May 4, 1993.)